Inorganic Chemistry

Article

pubs.acs.org/IC

Syntheses and Structures of $Sc_2Nb_{4-x}Sn_5$, YNb_6Sn_6, and $ErNb_6Sn_5$: Exploratory Studies in Ternary Rare-Earth Niobium Stannides

Cheng-Yang Yue[†,‡] and Xiao-Wu Lei*[,†,‡]

[†]Department of Chemistry and Chemical Engineering, Jining University, Qufu, Shandong 273155, People's Republic of China

[‡]State Key Laboratory of Structural Chemistry, Fujian Institute of Research on the Structure of Matter, Chinese Academy of Sciences, Fuzhou 350002, People's Republic of China

Supporting Information

ABSTRACT: Three new rare-earth (RE) niobium stannides, namely, $Sc_2Nb_{4-x}Sn_5$ (x = 0.37, 0.52), YNb_6Sn_6, and $ErNb_6Sn_5$, have been obtained by reacting the mixture of corresponding pure elements at high temperature and structurally characterized by single-crystal X-ray diffraction studies. $Sc_2Nb_{4-x}Sn_5$ crystallizes in the orthorhombic space group *Ibam* (No. 72) and belongs to the V_6Si_5 type. Its structure features a three-dimensional (3D) network composed of two-dimensionally (2D) corrugated $[Nb_2Sn_2]$ and $[Nb_2Sn_3]$ layers interconnected via Nb−Sn bonds, forming one type of one-dimensional (1D) narrow tunnels along the c axis occupied by Sc atoms. YNb_6Sn_6 crystallizes in the hexagonal space group *P6/mmm* (No. 191) and adopts the $HfFe_6Ge_6$ type, and $ErNb_6Sn_5$ crystallizes in the trigonal space group $R\bar{3}m$ (No. 166) and belongs to the $LiFe_6Ge_5$ type. Their structures both feature 3D networks based on 2D $[Nb_3Sn]$, $[Sn_2]$, and $[RESn_2]$ layers (RE = Y, Er). In YNb_6Sn_6, one type of $[Nb_3Sn]$ layer is interconnected by $[Sn_2]$ and $[YSn_2]$ layers via Nb−Sn bonds to form a 3D network. However, in $ErNb_6Sn_5$, two types of $[Nb_3Sn]$ layers are interlinked by $[Sn_2]$ and $[ErSn_2]$ layers via Nb−Sn bonds into a 3D framework. Electronic structure calculations and magnetic property measurements for "$Sc_2Nb_4Sn_5$" and YNb_6Sn_6 indicate that both compounds show semimetallic and temperature-independent diamagnetic behavior.

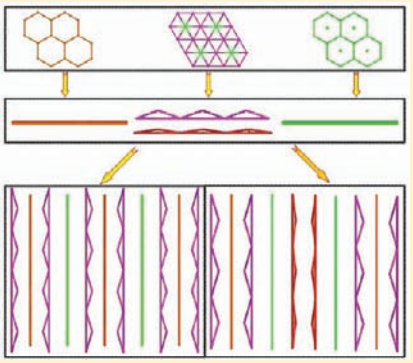

INTRODUCTION

The binary intermetallics of the Sn element with one electropositive alkali (or alkaline-earth metal) have been investigated intensively in the past several decades because of their remarkable structural diversity, novel chemical bonding, and manifold physical properties.[1−3] Many types of anionic Sn oligomers, chains, clusters, and nets have been found in these binary phases. Furthermore, ternary Sn-rich phases containing two types of cations with different sizes or charges exhibit various unusual anionic clusters or clathrate cages and possess interesting physical properties.[4−6]

In recent years, systematic research efforts in this area have resulted in the extension of these systems to include all rare-earth elements as well as most of the transition metals.[7−11] Such a design strategy has led to a very large family of ternary stannides with various structural types.[12−17] Especially, Pauling's electronegativities of transition metals are close to that of Sn, which always enable strong covalent bonding interactions between these elements. Hence, the introduction of transition metals in the binary phases can dramatically change their bonding character and structural type.[18−21] For example, the equiatomic ScTSn (T = Cu, Ag, Au) phases adopt LiGaGe ($P6_3mc$), TiFeSi ($I2cm$), and MgAgAs ($F\bar{4}3m$) type structures, respectively.[22] Similarly, ScNiSn crystallizes in the orthorhombic space group *Pnma* and adopts TiNiSi-type structure,[8] whereas ScPdSn and ScPtSn belong to the HfRhSn type ($P\bar{6}2c$).[23] Besides structural decoration, the abundant d orbital electrons of transition metals are also capable of greatly regulating the electronic and physical properties of the resultant compounds as well as improving their thermal stabilities. For instance, $Ce_3T_4Sn_{13}$ and $La_3T_4Sn_{13}$ (T = Co, Rh, Ir) phases feature multifarious physical properties in spite of the same type of structure.[24−26]

Among these ternary stannides, those containing a late transition metal (such as Mn, Co, Ni, Cu, and Zn) are now relatively well-known; however, reports on those containing Nb metal are still comparatively scarce. Phase diagram studies indicate that the binary Nb−Sn system exhibits three intermediate phases, namely, Nb_3Sn, Nb_6Sn_5, and $NbSn_2$, which show diversiform chemical-bonding character and intriguing physical properties.[27a] Especially, the cubic A15-type Nb_3Sn is considered to be one of the best candidates for superconducting wires because of its high critical temperature of 18.3 K and possibility to carry very large current densities far beyond the limits of the commonly used NbTi.[27b] Intrigued by the rich structural types and novel physical properties of these binary Nb−Sn phases, we undertook systematic studies in the ternary RE−Nb−Sn phases (RE = rare-earth metals), and so far only one compound of $TbNb_6Sn_6$ has been reported.[28] Our exploratory studies led to a series of new rare-earth niobium stannides, $Sc_2Nb_{4-x}Sn_5$ (x = 0.37, 0.52), YNb_6Sn_6, and

Received: November 9, 2011
Published: February 2, 2012

   dx.doi.org/10.1021/ic202414h | *Inorg. Chem.* 2012, 51, 2461−2471

$ErNb_6Sn_5$. They all feature three-dimensional (3D) networks based on Nb−Nb, Nb−Sn, and Sn−Sn bonds. Herein, we report their syntheses, crystal structures, band structures, and physical properties.

EXPERIMENTAL SECTION

Materials and Instruments. All manipulations were performed within an argon-filled glovebox with a moisture level below 1 ppm, although the title compounds were subsequently found to be stable in moist air for several months. All elements for the syntheses were used as received: rare-earth (RE) blocks (Acros, 99.99%), Nb powder (Tianjin Fuchen chemical reagent company, 99.99%), and Sn granules (Acros, 99.99%). Semiquantitative elemental analyses for RE, Nb, and Sn atoms were performed on a JSM-6700F scanning electron microscope equipped with an energy-dispersive spectroscopy detector. Powder X-ray diffraction (XRD) patterns were collected at room temperature on a X'Pert-Pro diffractometer using Cu Kα radiation (λ = 1.5406 Å) in the 2θ range of 5−85° with a step size of 0.04° and a 10 s/step counting time. Magnetic susceptibility measurements were performed on a Quantum Design PPMS-9T magnetometer at a field of 5000 Oe in the temperature range of 5−300 K.

Preparation of $Sc_2Nb_{4-x}Sn_5$ (x = 0.37, 0.52). A single crystal of $Sc_2Nb_{4-x}Sn_5$ (x = 0.52) was initially obtained by the reaction of Sc, Nb, and Sn metals with a molar ratio of 1:2:10, and the large excess of Sn metal was used as the flux. The mixture was loaded into a Ta tube, which was subsequently arc-welded under an Ar atmosphere and sealed in a quartz tube under vacuum (~10^{-4} Torr). The quartz tube was then put into a high-temperature furnace, allowed to react at 980 °C for 10 days, and annealed at 800 °C for 6 days. Then it was cooled to room temperature at a rate of 0.1 °C/min. Prism-shaped single crystals were selected from the reaction products for structural analysis. To increase the yield of $Sc_2Nb_{4-x}Sn_5$ (x = 0.52), a reaction using the loading composition of 2:3.5:5 (Sc/Nb/Sn) was set up in other Ta tubes under the same reaction conditions, which led to another phase of $Sc_2Nb_{4-x}Sn_5$ (x = 0.37) besides $Sc_2Nb_{4-x}Sn_5$ (x = 0.52). Microprobe elemental analysis on clean surfaces of the single crystal indicated the presence of Sc, Nb, and Sn elements in molar ratios of 2.0(2):3.5(4):5.1(9) and 2.0(5):3.7(3):5.2(2) for $Sc_2Nb_{4-x}Sn_5$ (x = 0.52) and $Sc_2Nb_{4-x}Sn_5$ (x = 0.37), respectively, which were in agreement with the results from single-crystal XRD studies. After the proper structural and composition analyses, the compound was prepared rationally in a high yield and high purity by reacting the mixture of the pure metals according to the loading composition of "$Sc_2Nb_4Sn_5$". A successful temperature profile entailed heating at 1000 °C for 8 days, annealing at 850 °C for 10 days, and slowly cooling to room temperature. The purity of the sample was confirmed by the powder XRD studies (see the Supporting Information).

Preparation of YNb_6Sn_6. Single crystals of YNb_6Sn_6 were first synthesized by reacting the mixture of Y, Nb, and Sn metals in a molar ratio of 2:4:5 during our attempts to prepare the Y analogue of $Sc_2Nb_{4-x}Sn_5$. The sample was reacted at 980 °C for 10 days and annealed at 800 °C for 6 days. Prism-shaped silvery white single crystals of YNb_6Sn_6 were selected from the reaction products for structural analysis. Microprobe elemental analyses on several single crystals indicated the presence of Y, Nb, and Sn elements in a molar ratio of 1.1(3):5.9(5):6.1(2), which was in agreement with the results derived from single-crystal XRD refinement. Subsequently, the reactions were carried out with a stoichiometric mixture of the corresponding elements in a Ta tube. The sample was heated at 1050 °C for 8 days and annealed at 770 °C for 8 days, and then it was allowed to slowly cool to room temperature. The measured powder XRD pattern agreed well with that simulated from the single-crystal X-ray structural analysis (see the Supporting Information).

Preparation of $ErNb_6Sn_5$. The $ErNb_6Sn_5$ compound was initially obtained by the direct combination of Er, Nb, and Sn metals in a molar ratio of 2:4:5 in our attempts to prepare Er analogue of $Sc_2Nb_{4-x}Sn_5$ under similar conditions. After the reaction, a small amount of the prism-shaped silvery white single crystals of $ErNb_6Sn_5$ were selected for structural and microprobe elemental analyses. The measured chemical composition, $Er_{0.9(2)}Nb_{5.8(7)}Sn_{5.1(2)}$, is in good agreement with those determined by single-crystal XRD studies. After the structure of $ErNb_6Sn_5$ was established, many efforts were subsequently made to prepare the single phase by reacting the stoichiometric mixtures of the pure elements in Ta tubes. The samples were heated at 1000 °C for 8 days, annealed at different temperatures (700, 800, 850, 900, and 950 °C, respectively, for each reaction) for 10 days, and then slowly cooled to room temperature. However, only a small amount of the prism-shaped crystals of $ErNb_6Sn_5$ were found, and powder XRD patterns revealed the presence of many impurity phases, such as Sc_5Sn_3, Sc, or Nb elements. The highest yield of about 30% for $ErNb_6Sn_5$ was obtained by annealing the sample at 850 °C. A number of attempts to synthesize other rare-earth analogues of the $Sc_2Nb_{4-x}Sn_5$, YNb_6Sn_6 and $ErNb_6Sn_5$ phases were also tried but were unsuccessful.

Crystal Structure Determination. Single crystals of $Sc_2Nb_{4-x}Sn_5$ (x = 0.37, 0.52), YNb_6Sn_6, and $ErNb_6Sn_5$ were selected from the reaction products and sealed into thin-walled glass capillaries within the glovebox. Data collections for all compounds were performed on the Rigaku Mercury CCD (Mo Kα radiation, graphite monochromator) at 293(2) K. All of the data sets were corrected for Lorentz factor, polarization, air absorption, and absorption because of variations in the path length through the detector faceplate. Absorption corrections based on the multiscan method were also applied.[29a]

All of the structures were solved using direct methods (*SHELXTL*) and refined by full-matrix least squares with atomic coordinates and anisotropic thermal parameters.[29b] For $Sc_2Nb_{4-x}Sn_5$ (x = 0.37, 0.52), inspection of the systematic absences for the full data sets indicated the possible space group to be *Ibam* (No. 72) or *Iba*2 (No. 45). The mean $|E^2 - 1|$ value of 0.883 was suggestive of a centrosymmetric space group; hence, *Ibam* was used for structural refinement and gave a satisfactory result. Site-occupancy refinements indicated that all sites were fully occupied except the Nb2 site with occupancy factors of 0.81(7) and 0.73(9) for $Sc_2Nb_{4-x}Sn_5$ (x = 0.37, 0.52), respectively. Final difference Fourier maps showed featureless residual peaks of 0.46 e Å^{-3} (0.76 Å from the Nb1 atom) and −0.47 e Å^{-3} (1.18 Å from the Sn1 atom) for $Sc_2Nb_{4-x}Sn_5$ (x = 0.37) and 2.09 e Å^{-3} (1.42 Å from the Sn3 atom) and −0.91 e Å^{-3} (0.90 Å from the Sn3 atom) for $Sc_2Nb_{4-x}Sn_5$ (x = 0.52). The space groups for YNb_6Sn_6 and $ErNb_6Sn_5$ were determined to be $P6/mmm$ (No. 191) and $R\bar{3}m$ (No. 166), respectively, based on systematic absences, E-value statistics, and satisfactory refinements. Site-occupancy refinements for these compounds indicated that all sites were fully occupied. Final difference Fourier maps showed featureless residual peaks of 1.45 e Å^{-3} (1.62 Å from the Sn1 atom) and −1.26 e Å^{-3} (0.94 Å from the Y1 atom) for YNb_6Sn_6 and 2.16 e Å^{-3} (1.42 Å from the Er1 atom) and −1.57 e Å^{-3} (0.86 Å from the Sn1 atom) for $ErNb_6Sn_5$. Data collection and refinement parameters are summarized in Table 1. Atomic coordinates and important bond lengths are listed in Tables 2 and 3, respectively. More details about crystallographic studies and atomic displacement parameters are given in the Supporting Information.

Computational Details. To better understand the electronic structures of the title compounds, ab initio electronic structure calculations were carried out for YNb_6Sn_6 and idealized "$Sc_2Nb_4Sn_5$" models as representatives; in the latter, all of the Nb sites were assumed to be fully occupied. The calculations were performed with both the full-potential linearized augmented plane wave plus local basis (FPLAPW+lo) method (*WIEN2K*) and tight-binding linear muffin-tin orbital method (TB-LMTO).

WIEN2K. The *WIEN2K* program is based on the density functional theory and the highly accurate FPLAPW+lo method, using the generalized gradient approximation (GGA-PBE) to treat the exchange and correlation potential.[30] Within the FPLAPW method, the space is divided into nonoverlapping muffin-tin (MT) spheres and an interstitial region. In order to obtain results as precise as possible, we expanded the basis function up to $R_{MT}K_{MAX}$ = 7, where R_{MT} is the smallest MT spherical radius present in the system and K_{MAX} is the maximum modulus for the reciprocal lattice vector. We adopted the values of 2.5, 2.5, and 2.42 au for RE, Nb, and Sn atoms, respectively,

dx.doi.org/10.1021/ic202414h | *Inorg. Chem.* 2012, 51, 2461−2471

Table 1. Crystal Data and Structure Refinements for $Sc_2Nb_{4-x}Sn_5$ (x = 0.37), YNb_6Sn_6, and $ErNb_6Sn_5$

chemical formula	$Sc_2Nb_{3.63}Sn_5$	YNb_6Sn_6	$ErNb_6Sn_5$
fw	1021.10	1358.51	1318.17
space group	*Ibam* (No. 72)	*P6/mmm* (No. 191)	$R\bar{3}m$ (No. 166)
a (Å)	8.672(3)	5.7498(6)	5.7730(17)
b (Å)	18.719(6)	5.7498(6)	5.7730(17)
c (Å)	5.6645(16)	9.5003(15)	51.05(2)
V (Å^3)	919.6(5)	272.00(6)	1473.5(9)
Z	4	1	6
D_{calcd} (g cm^{-3})	7.376	8.294	8.913
temp (K)	293(2)	293(2)	293(2)
μ (mm^{-1})	18.963	24.757	27.538
GOF on F^2	1.171	1.013	1.259
R1, wR2 [$I > 2\sigma(I)$][a]	0.0094/0.0180	0.0156/0.0333	0.0228/0.0527
R1, wR2 (all data)	0.0105/0.0187	0.0176/0.0341	0.0249/0.0536

[a] $R1 = \sum||F_o| - |F_c||/\sum|F_o|$, $wR2 = \{\sum w[(F_o)^2 - (F_c)^2]^2/\sum w[(F_o)^2]^2\}^{1/2}$.

Table 2. Atomic Coordinates and Equivalent Isotropic Displacement Parameters (Å^2 × 10^3) for $Sc_2Nb_{4-x}Sn_5$ (x = 0.37), YNb_6Sn_6, and $ErNb_6Sn_5$

atom	Wyckoff	x	y	z	U(eq)[a]
		$Sc_2Nb_{4-x}Sn_5$ (x = 0.37)			
Sc1	8j	0.1104(1)	0.3541(1)	1/2	8(1)
Nb1	8g	0	0.1896(1)	1/4	5(1)
Nb2	8j	0.2605(1)	0.4335(1)	0	7(1)
Sn1	8j	0.2016(1)	0.2871(1)	0	6(1)
Sn2	8j	0.1024(1)	0.0673(1)	0	7(1)
Sn3	4a	0	1/2	1/4	8(1)
		YNb_6Sn_6			
Y1	1b	0	0	1/2	10(1)
Nb1	6i	1/2	0	0.2507(1)	4(1)
Sn1	2e	0	0	0.1705(1)	8(1)
Sn2	2c	2/3	1/3	0	6(1)
Sn3	2d	2/3	1/3	1/2	5(1)
		$ErNb_6Sn_5$			
Er1	6c	0	0	0.0894(1)	4(1)
Nb1	18h	0.1716(1)	0.3431(2)	0.1931(1)	5(1)
Nb2	18h	0.5003(1)	0.4997(1)	0.0469(1)	2(1)
Sn1	6c	0	0	0.1476(1)	3(1)
Sn2	6c	0	0	0.0295(1)	3(1)
Sn3	6c	0	0	0.3333(1)	3(1)
Sn4	6c	0	0	0.2398(1)	3(1)
Sn5	6c	0	0	0.5737(1)	3(1)

[a] U(eq) is defined as one-third of the trace of the orthogonalized U_{ij} tensor.

as the R_{MT} radii. In addition, we used a separate energy of −8.0 Ry between the valence and core states. Thus, the Sc 3d4s, Y 4d5s, Nb 4d5s, and Sn 5s5p orbitals were treated as valence states, while the Sc 3s3p, Y 4s4p, Nb 4s4p, and Sn 4p4d orbitals acted as semicore states with other electrons as core states. We calculated the total energy and magnetic moments with 100, 300, and 500 k points for both compounds, and the results suggested that the calculated results did not change much from 100 to 500 k points. Hence, in this study, we used 300 k points in the complete Brillouin zone, in which the integration was carried out with a modified tetrahedron method.[31] Convergence of the self-consistency calculation of the electronic structure was achieved when the total energy variation from iteration to iteration converged to be 0.01 mRy accuracy or better. The Fermi level was selected as the energy reference (E_F = 0 eV). Furthermore, to improve the description of the strongly correlated f and d electrons, we also introduced the on-site Coulomb energy U correction, namely, the GGA + U-type calculation.[32]

Table 3. Selected Bond Lengths (Å) for $Sc_2Nb_{4-x}Sn_5$ (x = 0.37), YNb_6Sn_6, and $ErNb_6Sn_5$

	$Sc_2Nb_{4-x}Sn_5$ (x = 0.37)		
Sc1−Sc2	2.894(1)	Sc1−Sn1	3.1968(8) × 2
Sc1−Sn1	2.982(1)	Sc1−Sn3	3.2225(9) × 2
Sc1−Sn1	3.105(1)	Sc1−Nb1	3.521(1) × 2
Sc1−Nb2	3.4539(8) × 2	Nb2−Sn2	2.7716(8)
Nb1−Nb1	2.8322(8) × 2	Nb2−Sn1	2.7879(9)
Nb1−Sn1	2.8973(6) × 2	Nb2−Sn3	2.9426(7) × 2
Nb1−Sn1	2.9820(8) × 2	Nb2−Sn2	2.965(1)
Nb1−Sn2	2.8349(7) × 2	Nb2−Sn2	3.0717(8) × 2
Sn1−Sn1	3.2641(8) × 2	Sn3−Sn3	2.8322(8) × 2
Sn2−Sn2	3.0815(8)		
	YNb_6Sn_6		
Y1−Sn1	3.131(1) × 2	Y1−Sn3	3.3196(4) × 4
Nb1−Nb1	2.8749(3) × 4	Y1−Sn3	3.3196(3) × 2
Nb1−Sn3	2.8918(6) × 2	Sn1−Sn1	3.239(2)
Nb1−Sn2	2.9034(6) × 2	Sn2−Sn2	3.3197(3) × 3
Nb1−Sn1	2.9744(4) × 2	Sn3−Sn3	3.3197(3) × 3
	$ErNb_6Sn_5$		
Er1−Sn1	2.972(2)	Er1−Sn4	3.340(1) × 3
Er1−Sn2	3.060(2)	Er1−Nb2	3.611(1) × 6
Er1−Sn5	3.338(1) × 3	Nb2−Nb2	2.882(1) × 2
Nb1−Nb1	2.802(2) × 2	Nb2−Nb2	2.891(2) × 2
Nb1−Nb1	2.971(2) × 2	Nb2−Sn5	2.883(1)
Nb1−Sn1	2.886(1)	Nb2−Sn4	2.904(1)
Nb1−Sn5	2.906(1)	Nb2−Sn3	2.916(1)
Nb1−Sn1	2.9113(9)	Nb2−Sn3	2.920(1)
Nb1−Sn1	2.9114(9)	Nb2−Sn2	3.0205(9) × 2
Nb1−Sn4	2.938 (1)	Sn2−Sn2	3.010(2)
Sn3−Sn3	3.333(1)	Sn4−Sn5	3.333(1)

Stuttgart LMTO Program. This program follows the TB-LMTO method in the local density approximation.[33] All relativistic effects except for spin−orbit coupling were taken into account by the scalar relativistic approximation.[34] Interstitial spheres were introduced in the latter to achieve space filling. The atomic sphere approximation radii as well as the positions and radii of additional empty spheres were calculated automatically. The basis set included the 4s, 4p, 3d, and 3f orbitals for the Sc atom and the 5s, 5p, 4d, and 4f orbitals for the Y, Nb, and Sn atoms. The Sc 3f, Y 4f, Nb 4f, and Sn 4d4f orbitals were treated with the downfolding technique.[35] In both cases, the k-space integrations were performed by the tetrahedron method.[31] The Fermi level was selected as the energy reference (E_F = 0 eV).

RESULTS AND DISCUSSION

Crystal Structures. Our exploratory studies in the ternary RE−Nb−Sn system led to three new compounds, namely, $Sc_2Nb_{4-x}Sn_5$ (x = 0.37, 0.52), YNb_6Sn_6, and $ErNb_6Sn_5$. Their structures all feature 3D networks based on Nb−Nb, Nb−Sn, and Sn−Sn bonds.

The structure of $Sc_2Nb_{4-x}Sn_5$ belongs to the V_6Si_5 type, which is also adopted by several ternary transition-metal silicides, such as $R_2Cr_4Si_5$ (R = Sc, Ti, Zr, Hf, Nb, Ta), $R_2V_4Si_5$ (R = Nb, Ta), $R_2Mn_4Si_5$ (R = Ti, Nb, Ta), and $Cr_2Nb_4Si_5$.[36] In these ternary phases, group 14 elements always occupy the Si position of V_6Si_5, and two types of transition metals are available to replace three different V sites of V1, V2, and V3 with various manners. Generally speaking, the earlier transition

dx.doi.org/10.1021/ic202414h | Inorg. Chem. 2012, 51, 2461−2471

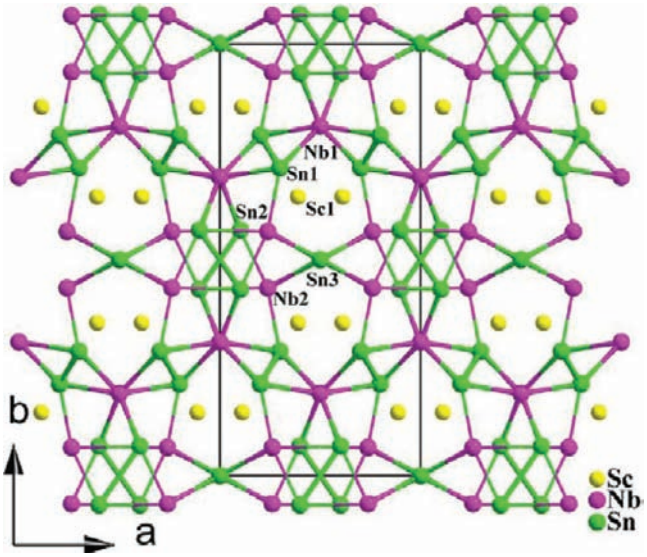

Figure 1. General view of the structure of $Sc_2Nb_{4-x}Sn_5$ (x = 0.37) along the c axis. The Sc, Nb, and Sn atoms are drawn as yellow, purple, and green spheres, respectively. The unit cell is outlined.

metal of smaller Pauling's electronegativity and larger atomic size commonly occupies the V1 site, whereas the later transition metal of larger Pauling's electronegativity and smaller atomic size currently replaces the V2 and V3 positions, such as $R_2Cr_4Si_5$ (R = Sc, Ti, Zr, Hf, Nb) and $Sc_2Nb_{4-x}Sn_5$ with compositions of $R_2[Cr_2Cr_2]Si_5$ and $Sc_2[Nb_{2-x}Nb_2]Sn_5$, respectively.[36c] However, the larger atoms also tend to occupy the V3 site and the smaller atoms replace the V1 and V2 sites when these transition metals have approximative Pauling's electronegativities, such as $R_2V_4Si_5$ (R = Nb, Ta), $R_2Mn_4Si_5$ (R = Ti, Nb, Ta), and $Ta_2Cr_4Si_5$ with compositions of $V_2[V_2R_2]Si_5$, $Mn_2[Mn_2R_2]Si_5$, and $Cr_2[Cr_2Ta_2]Si_5$, respectively.

The general view of $Sc_2Nb_{4-x}Sn_5$, in Figure 1, illustrates the 3D framework, which is composed of two-dimensionally (2D) corrugated $[Nb_2Sn_2]$ and $[Nb_2Sn_3]$ layers interconnected via Nb−Sn bonds, forming one-dimensional (1D) narrow tunnels along the c axis occupied by Sc atoms. Because both of the $Sc_2Nb_{4-x}Sn_5$ compounds are isostructural, the structure of

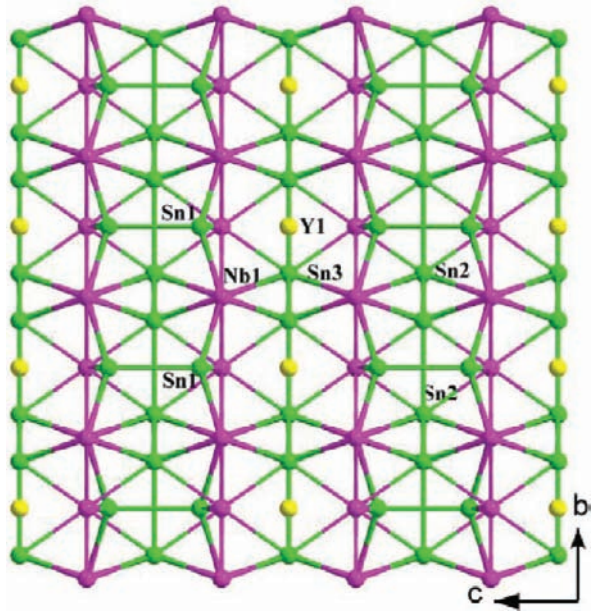

Figure 3. General view of the hexagonal structure of YNb_6Sn_6 along the a axis. The Y, Nb, and Sn atoms are drawn as yellow, purple, and green spheres, respectively.

$Sc_2Nb_{4-x}Sn_5$ (x = 0.37) will be discussed in detail as a representative.

As shown in Figure 2a, the 2D corrugated $[Nb_2Sn_2]$ layer is formed by a 1D linear Nb chain and a zigzag Sn chain interconnected via Nb1−Sn1 bonds. In the linear Nb chain, the Nb1−Nb1 distance of 2.8322(8) Å is slightly shorter than the sum of the covalent radii of 2.834 Å,[37] showing strong covalent Nb−Nb bonding (Figure 2b). It should be noted that the 1D zigzag Sn chain containing equal Sn1−Sn1 distances is slightly different from that reported in Yb_3CoSn_6, in which the zigzag Sn chain features inequable Sn−Sn distances.[38] A similar 2D $[Nb_2Sn_2]$ layer has also been reported in $NbSn_2$, which is also composed of a 1D linear Nb chain and a zigzag Sn chain.[27] In $Sc_2Nb_{4-x}Sn_5$, the neighboring zigzag Sn chains are wavily bridged by the Nb chain to form a corrugated $[Nb_2Sn_2]$ layer,

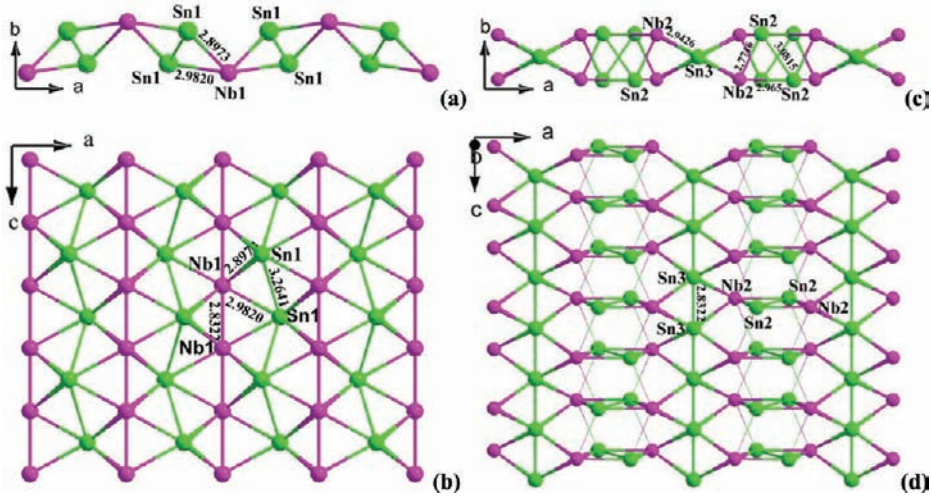

Figure 2. Closeup view of the section of the 2D $[Nb_2Sn_2]$ layer in $Sc_2Nb_{4-x}Sn_5$ (x = 0.37) along the c axis (a) and the b axis (b) and the 2D $[Nb_2Sn_3]$ layer along the c axis (c) and the b axis (d).

dx.doi.org/10.1021/ic202414h | Inorg. Chem. 2012, 51, 2461−2471

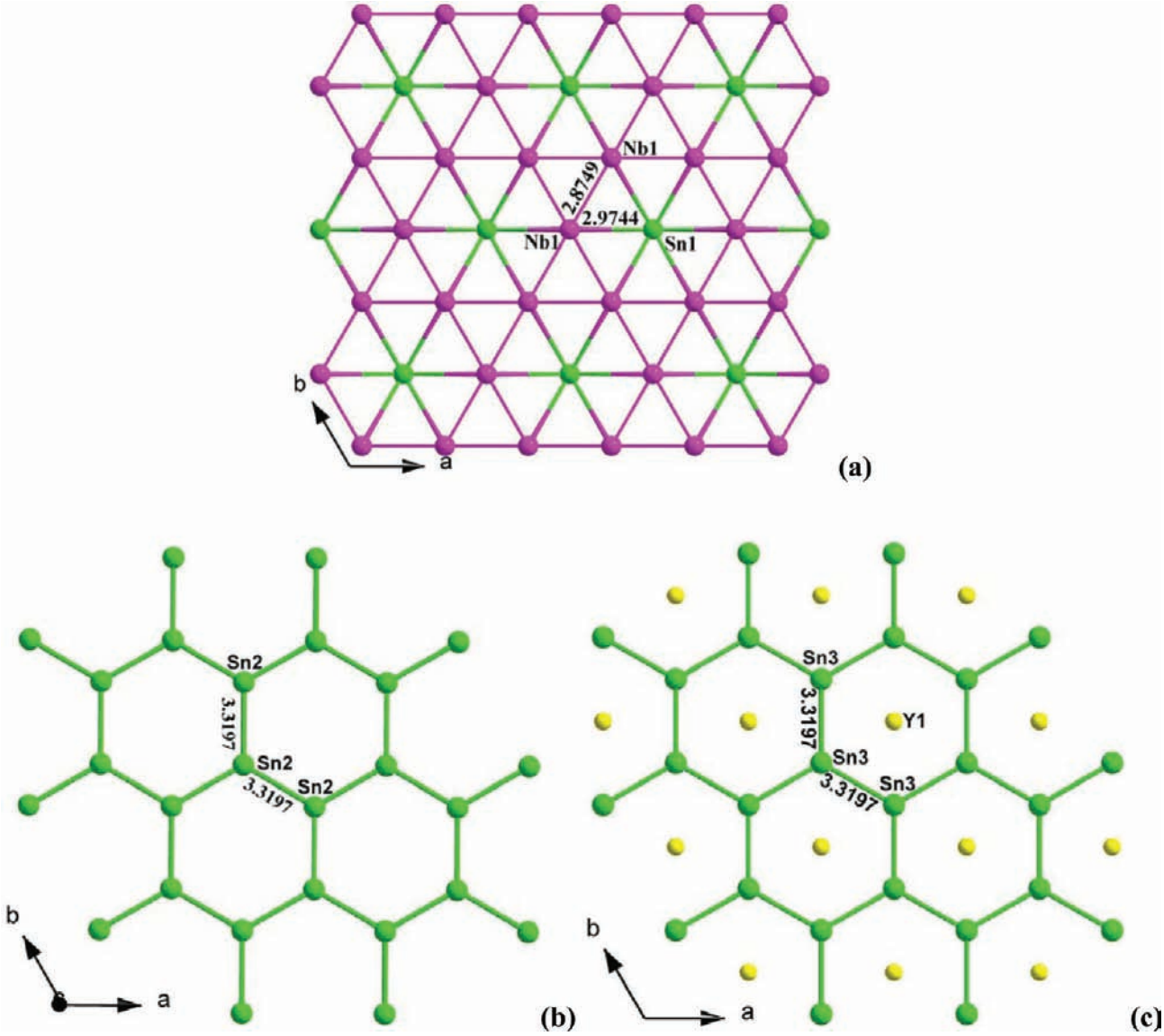

Figure 4. Detailed view of the 2D $[Nb_3Sn]$ layer (a), $[Sn_2]$ layer (b), and $[YSn_2]$ layer (c) along the *c* axis in YNb_6Sn_6.

whereas they are interconnected in a parallel manner to form a flat $[Nb_2Sn_2]$ layer in $NbSn_2$.

The basic building blocks of the 2D $[Nb_2Sn_3]$ layer are a parallelogram-shaped $[Nb_2Sn_2]$ unit and a 1D linear Sn chain, as shown in Figure 2c. The parallel $[Nb_2Sn_2]$ units of the Nb2 and Sn2 atoms are reversely interlinked via weak Nb2−Sn2 bonds [3.0717(8) Å] to form a 1D $[Nb_2Sn_2]$ chain along the *c* axis and are bridged by a linear Sn chain of Sn3 atoms via Nb2−Sn3 bonds into the 2D $[Nb_2Sn_3]$ layer parallel to the *ac* plane (Figure 2d).

The 2D $[Nb_2Sn_2]$ and $[Nb_2Sn_3]$ layers are further joined together via Nb1−Sn2 and Nb2−Sn1 bonds to form a 3D $[Nb_4Sn_5]$ framework with long narrow tunnels composed of $[Nb_3Sn_3]$ six-membered rings along the *c* axis, which are occupied by the Sc1 atoms (Figure 1). The Sc1 atom is surrounded by four Nb and seven Sn atoms with Sc−Nb and Sc−Sn distances in the ranges of 3.4539(8)−3.521(1) and 2.894(1)−3.2225(9) Å, respectively. The Nb1 atom is in close contact with two Nb1, two Sn2, and four Sn1 atoms, whereas the Nb2 atom is seven-coordinated by one Sn1, four Sn2, and two Sn3 atoms. Most of the Nb−Sn bonds have a rather narrow range of 2.7716(8)−2.965(1) Å, which is comparable with the sum of the covalent radii of 2.835 Å,[37] indicating strong covalent Nb−Sn bonding (Figure S1 in the Supporting Information). All of the Sn−Sn bond distances are in the range of 2.8322(8)−3.2641(8) Å, which is in accordance with those reported in Yb_3CoSn_6, Sm_2NiSn_4, $Yb_5Ni_4Sn_{10}$, $Yb_7Ni_4Sn_{13}$, etc.[38]

The structure of YNb_6Sn_6 belongs to the $HfFe_6Ge_6$ type, which is also known for many other relevant ternary phases, such as $REMn_6Sn_6$ (RE = rare earth atoms), RFe_6Ge_6 (R = Ti, Zr, Nb, Sc, Y, Lu), RCo_6Ge_6 (R = Mg, Ti, Zr, Hf), $RECr_6Ge_6$ (RE = Tb, Dy, Ho, Er), etc.[39,40] Its structure features a 3D network based on three types of 2D infinite layers: $[Nb_3Sn]$, $[Sn_2]$, and $[YSn_2]$ layers, which are interconnected via Nb−Sn and Sn−Sn bonds along the *c* axis (Figure 3).

There are one Y, one Nb, and three Sn atoms in the asymmetric unit of YNb_6Sn_6. In Figure 4a, all of the regular $[Nb_6]$ hexagons of the Nb1 atom are capped by Sn1 atoms on one side and further condensed via corner sharing into a 2D $[Nb_3Sn]$ layer. The Sn1 atom is 0.763 Å off the plane formed by the $[Nb_6]$ hexagon. Similar capped hexagonal sheets have

dx.doi.org/10.1021/ic202414h | *Inorg. Chem.* 2012, 51, 2461−2471

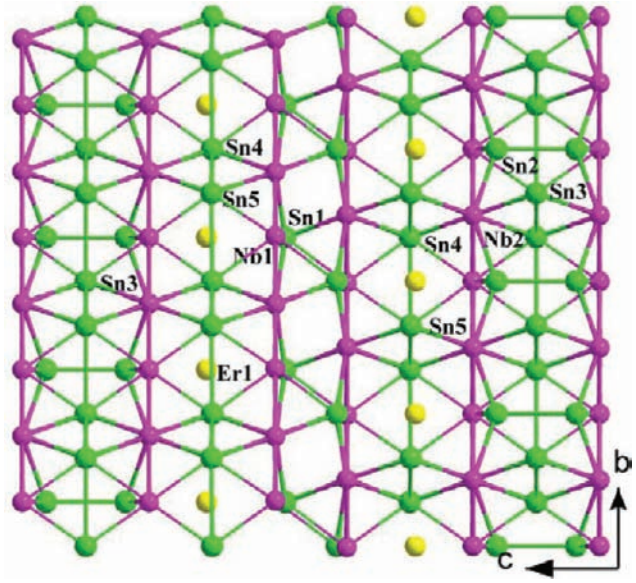

Figure 5. Perspective view of the part structure of $ErNb_6Sn_5$ viewed down the *a* axis. The Er, Nb, and Sn atoms are shown as yellow, purple, and green spheres, respectively.

also been reported for $[Mn_3Sn]$ layer in $REMn_6Sn_6$ and $[Co_3Ge]$ layer in $MgCo_6Ge_6$.[39,40] The Sn2 atoms form a 2D planar graphite-type $[Sn_2]$ layer arising from the condensation of regular $[Sn_6]$ hexagons via edge sharing, which is similar to those in $NbSn_2$ and $REMn_6Sn_6$.[27,39] The Sn2−Sn2 distance of 3.3197(3) Å is longer than the corresponding Sn−Sn distances (3.160−3.206 Å) of $[Sn_6]$ hexagons in $REMn_6Sn_6$ (RE = Sc, Y, Nd, Sm, Tb, Ho, Tm).[39] Such a Sn−Sn distance is close to those reported in the Sn square sheets of Yb_3CoSn_6 and $BaMg_2Sn_2$, which could be considered as a weak bonding interaction.[38,41] The Sn3 atoms also form the same 2D planar $[Sn_2]$ layer as that of the Sn2 atoms with a Sn3−Sn3 distance of 3.3197(3) Å. It is different that all of the Y atoms are sitting in the center of $[Sn_6]$ hexagons of Sn3 atoms to form 2D $[YSn_2]$ layers but not for Sn2 atoms (Figure 4c).

These 2D $[Nb_3Sn]$, $[Sn_2]$, and $[YSn_2]$ layers are further joined together via Nb−Sn bonds along the *c* axis into the 3D YNb_6Sn_6 network (Figure 3). Such connectivity also results in a short interlayer Sn1−Sn1 distance of 3.239(2) Å, which is shorter than the intralayer Sn−Sn distance of 3.3197(3) Å. The Y1 atom is coordinated by two Sn1 and six Sn3 atoms with Y−Sn distances in the range of 3.131(1)−3.3196(4) Å, which are comparable with those reported in $Y_7Co_6Sn_{23}$ and YMSn (M = Cu, Ag, Au).[16a,22,42] Its coordination geometry can be described as a hexagonal bipyramid. The Nb1 atom is surrounded by four Nb and six Sn atoms with Nb−Nb and Nb−Sn distances of 2.8749(3) and 2.8918(6)−2.9744(4) Å, respectively, which are comparable with those in $Sc_2Nb_{4-x}Sn_5$ (Figure S3 in the Supporting Information). It is found that most of the Nb−Nb, Nb−Sn, and Sn−Sn bond lengths in YNb_6Sn_6 are slightly shorter than those of $TbNb_6Sn_6$, which is in accordance with the radii of RE ions.

$ErNb_6Sn_5$ is isostructural to $LiFe_6Ge_5$, with the Er atom filling the Li site, Nb atoms replacing Fe sites, and Sn atoms corresponding to Ge positions.[43] Its structure features a 3D network based on two types of 2D $[Nb_3Sn]$ layers as well as planar $[Sn_2]$ and $[ErSn_2]$ layers interconnected via Nb−Sn and Sn−Sn bonds (Figure 5). Its structure contains one Er, two Nb, and five Sn atoms in the asymmetric unit. The Nb1 and Sn1 atoms form the first type of $[Nb_3Sn]$ layer, and the Nb2 and Sn2 atoms construct the second kind of $[Nb_3Sn]$ layer in a manner similar to that of YNb_6Sn_6 (Figure 6a,b). The Sn1 and Sn2 atoms are 0.376 and 0.889 Å off the plane formed by $[Nb_6]$ hexagons, respectively. Within each type of $[Nb_3Sn]$ layer, two types of Nb−Nb bonds are found: 2.802(2) and 2.971(2) Å for the first and 2.882(1) and 2.891(2) Å for the second, which are different from the $[Nb_3Sn]$ layer of YNb_6Sn_6 with an equal Nb−Nb distance of 2.8749(3) Å. The 2D planar $[Sn_2]$ layer is formed by the Sn3 atom, and the $[ErSn_2]$ layer is made up of Er1, Sn4, and Sn5 atoms, where the connecting manners are also in accordance with those of YNb_6Sn_6. Both Sn3−Sn3 and Sn4−Sn5 distances of 3.333 Å are greatly close to those in YNb_6Sn_6.

All of the 2D $[Nb_3Sn]$, $[Sn_2]$, and $[ErSn_2]$ layers are interlinked via Nb−Sn bonds along the *c* axis to form a 3D $ErNb_6Sn_5$ network (Figure 5). Such connectivity also leads to a short interlayer Sn2−Sn2 distance of 3.010(2) Å, which is evidently shorter than the corresponding bond distance in YNb_6Sn_6 [3.239(2) Å]. In $ErNb_6Sn_5$, the Er1 atom is surrounded by six Nb2, one Sn1, one Sn2, three Sn4, and three Sn5 atoms with Er−Nb and Er−Sn distances of 3.611(1) and 2.972(2)−3.340(1) Å, respectively. The Nb1 atom is nine-coordinated by four Nb and five Sn atoms, whereas the Nb2 atom closely contacts with four Nb and six Sn atoms. The Nb−Sn distances fall in the range of 2.883(1)−3.0205(9) Å, which is close to those in $Sc_2Nb_{4-x}Sn_5$ and YNb_6Sn_6.

The most prominent features for YNb_6Sn_6 and $ErNb_6Sn_5$ are the manifold 2D layers as well as their connecting manners. Their structures both feature 3D networks based on three types of 2D layers: $[Nb_3Sn]$, $[Sn_2]$, and $[RESn_2]$ (RE = Y, Er) layers with the same structural conformation. In YNb_6Sn_6, there is only one sort for each type of $[Nb_3Sn]$, $[Sn_2]$, and $[YSn_2]$ layer, marked as A, B, and C types, respectively, for convenient descriptions. However, in $ErNb_6Sn_5$, there are two types of similar $[Nb_3Sn]$ layers and one sort for respective $[Sn_2]$ and $[ErSn_2]$ layer, marked as A, A′, B, and C types, respectively. Furthermore, these 2D layers feature different stacking orders. In YNb_6Sn_6, the A, B, and C layers are interconnected according to $^{\infty}$[A−B−A−C] order along the *c* axis to form a 3D network (Figure 7a), whereas the A, A′, B, and C layers are interlinked according to the sequence of $^{\infty}$[A−B−A−C−A′−A′−C] along the *c* axis into a 3D network in $ErNb_6Sn_5$ (Figure 7b). Such structural characters of YNb_6Sn_6 and $ErNb_6Sn_5$ based on 2D layers are also homologous to the structures of some binary vanadium family element tetrelides. For example, the 3D structure of MSn_2 (M = V, Nb, Ta) is composed of a 2D $[M_2Sn_2]$ layer and a graphite-type $[Sn_2]$ layer (B-type), and MTt_2 (M = V, Nb, Ta; Tt = Si, Ge) features 3D networks based on a transitional-metal-centered $[MTt_2]$ layer (C type). The 3D structures of YNb_6Sn_6 and $ErNb_6Sn_5$ can also be considered as the intergrowth of different types of 2D slabs.[44] As shown in Figure S4a in the Supporting Information, the structure of YNb_6Sn_6, referred to as the $HfFe_6Ge_6$ type, is built up from an alternating stacking of Zr_4Al_3- and $CaCu_5$-type slabs. The structure of $ErNb_6Sn_5$ ($LiFe_6Ge_5$ type) contains structural slabs, characteristic of the $HfFe_6Ge_6$ type, in which each Zr_4Al_3-type layer is surrounded by a $CaCu_5$-type layer on each side similar to that in YNb_6Sn_6. The $HfFe_6Ge_6$- and $PuGa_3$-type slabs further alternately stack along the *c* axis to form a 3D framework (Figure S4b in the Supporting Information).

dx.doi.org/10.1021/ic202414h | *Inorg. Chem.* 2012, 51, 2461−2471

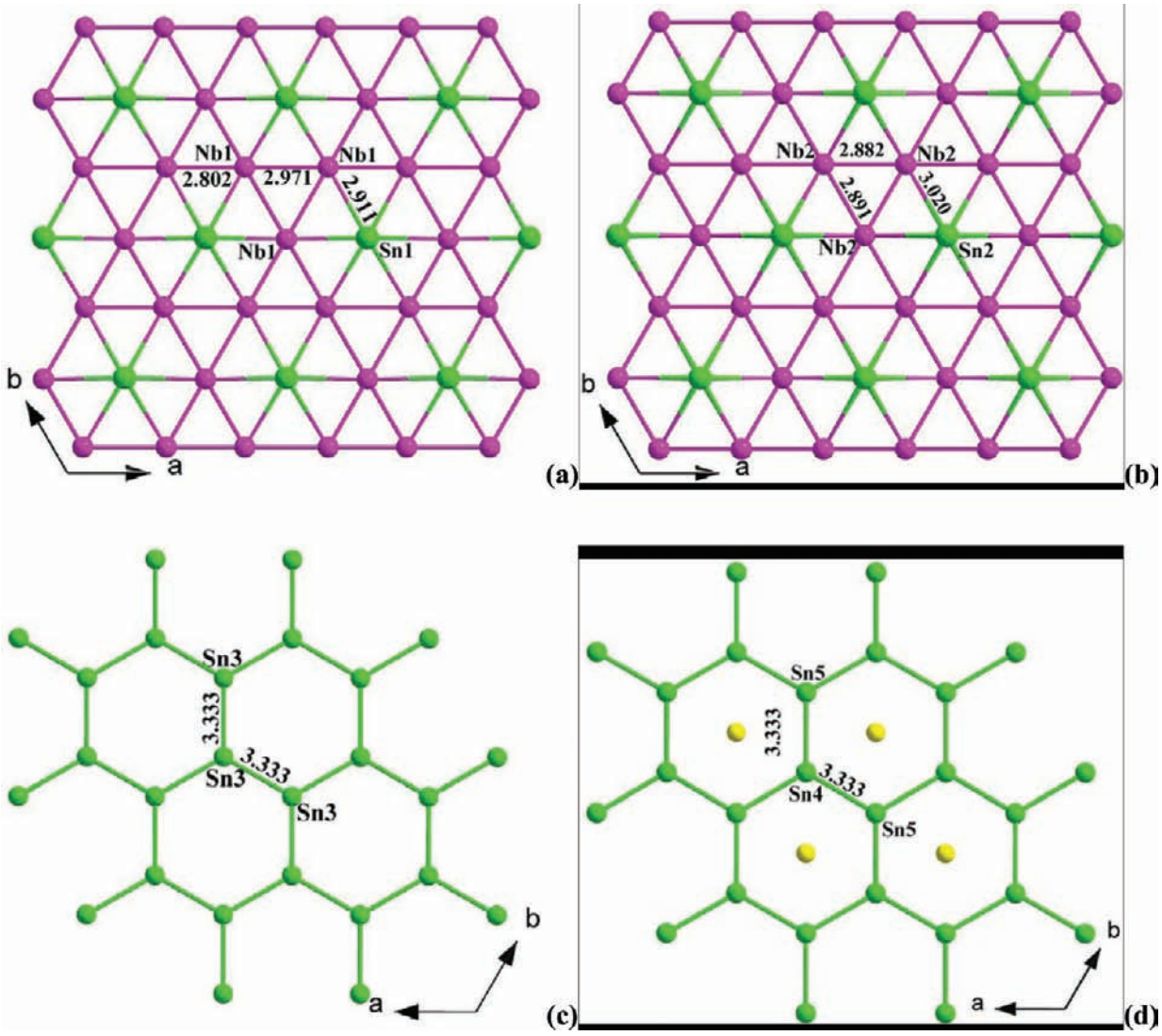

Figure 6. Fragments of two types of 2D $[Nb_3Sn]$ layers (a and b) and the $[Sn_2]$ layer (c) and $[ErSn_2]$ layer (d) viewed down the *c* axis in $ErNb_6Sn_5$.

Magnetic Properties. To assess the physical properties of "$Sc_2Nb_4Sn_5$" and YNb_6Sn_6, preliminary measurements of their magnetic properties have been made. Further work is necessary to understand how the level of Nb deficiency affects these properties for $Sc_2Nb_{4-x}Sn_5$. Plots of the molar magnetic susceptibility χ_m of "$Sc_2Nb_4Sn_5$" and YNb_6Sn_6 as a function of the temperature in the range of 5−300 K are presented in Figure S5 (Supporting Information). Both compounds exhibit essentially temperature-independent diamagnetic behavior over 10−300 K with susceptibilities of about -7.22×10^{-4} and -4.93×10^{-4} emu mol^{-1} for "$Sc_2Nb_4Sn_5$" and YNb_6Sn_6, respectively. The slight increase of the molar susceptibility below 10 K probably arises from the presence of minor amounts of paramagnetic impurities. The intrinsic diamagnetic behaviors of the compounds are consistent with the nonmagnetic characters of all of the metallic constituents. Such phenomena have also been observed in other phases containing Sc and Y, such as ScAuSn and YAuSn.[22]

Band Structure Calculations. To investigate the electronic properties of "$Sc_2Nb_4Sn_5$" and YNb_6Sn_6, we carried out accurate band structure calculations by using the FPLAPW method. The spin polarization was properly taken into account by considering the d-electron effect of the Nb atom, but no obvious spin splitting was observed in both compounds. The calculated total density of states (DOS) and partial DOS (PDOS) from each element with no spin polarization are shown in Figure 8. It is seen that their Fermi levels both fall in the pseudogap, in a region with low density of states, which indicates that the compounds show semimetallic behaviors. In both cases, the outer s and d states of RE atoms mainly locate above the Fermi level. Furthermore, the calculations converge to theoretical saturation moments of almost 0 μ_B for all of the RE atoms. Hence, all of the RE cations are most likely in oxidation states of 3+ in two compounds, which are in accordance with the results of magnetic measurements. In both cases, the Nb 4d bands are partially occupied and mostly localized in the range of −5 to +6 eV, and the PDOS of all of the Sn atoms spread over the whole energy range (5s, −10 to −6 eV; 5p, −5 to 0 eV) with larger dispersion. It is found that the strong Sn p/Nb d hybridization just below the Fermi level indicates the strong covalent character of the Nb−Sn bonds.

Furthermore, considering the local d and f electrons in these compounds, we further perform GGA + *U* (on-site Coulombic energy correction) type calculations to examine the correlation of d or f electrons. It is found that the DOS is unchanged except small quantitative changes for two compounds. Namely,

dx.doi.org/10.1021/ic202414h | *Inorg. Chem.* 2012, 51, 2461−2471

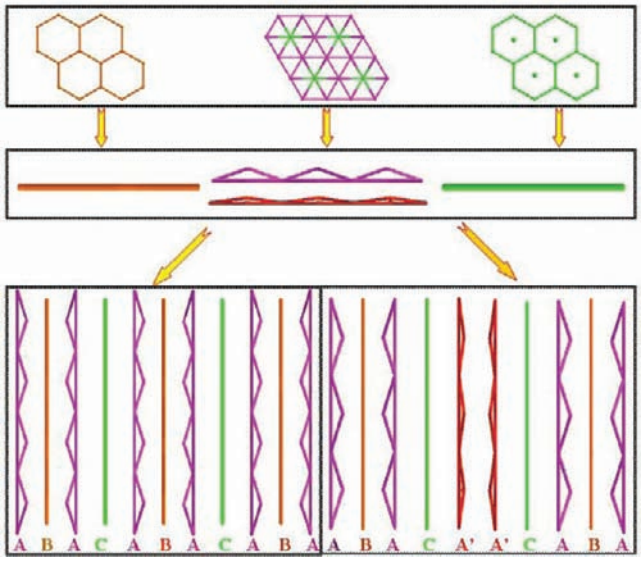

Figure 7. Schematic representation of the stacking manners of YNb_6Sn_6 (left) and $ErNb_6Sn_5$ (right) based on different types of 2D layers. The [Nb_3Sn] layer (A and A′ types), [Sn_2] layer (B type), and [$RESn_2$] layer (C type) are represented using purple, red, yellow, and green slabs, respectively. The Nb−Sn and Sn−Sn bonds among the 2D layers are deleted for clarity.

the *U* parameter does not influence the energy and DOS of both d and f electrons. Thus, the GGA exchange correlation formation can give sufficient and reliable results.

To further interpret the chemical bonding, the results of the TB-LMTO calculations have been utilized through crystal orbital Hamilton population (COHP) analyses because the *WIEN2K* code does not support such analyses (Figure 9). Furthermore, to quantify the interaction between atoms, integrated COHP (ICOHP) analyses were also determined, and the calculated values are listed in Tables S3 (Supporting Information). Such a calculation strategy has been effectively used in many cases.[45] In both cases, the Nb−Nb bonds [2.8322(8)−2.8749(3) Å] and Nb−Sn bonds [2.7716(8)−2.9744(4) Å] are effectively optimized at the Fermi level with large ICOHP values of 2.02−2.08 and 1.0−1.69 eV bond^{-1}, respectively, which indicate strong covalent Nb−Nb and Nb−Sn bonding interactions. However, in "$Sc_2Nb_4Sn_5$", the ICOHP value of 0.47 eV for the longer Nb−Sn bond [3.0717(8) Å] is relatively small, as expected, indicating that such a bond is much weaker than the shorter Nb−Sn bonds [2.7716(8)−2.9744(4) Å]. The Sn−Sn contacts show various bonding character depending on the different bond distances. The shorter Sn−Sn bond of 2.8322(8) Å in "$Sc_2Nb_4Sn_5$" with a ICOHP value of 1.03 eV is much stronger than the Sn−Sn bonds of 3.0815(8)−3.2641(8) Å in "$Sc_2Nb_4Sn_5$" and 3.3197(3) Å in YNb_6Sn_6 with ICOHP values of 0.36−0.58 and 0.28 eV bond^{-1}, respectively. It should be noted that some antibonding states below the Fermi level lead to a weakening of Sn−Sn bonding interactions, which has been investigated in detail elsewhere.[46] As expected, the Sc−Nb, Sc−Sn, and Y−Sn bonds are weakly bonding with small ICOHP values of about 0.11−0.19, 0.22−0.41, and 0.36−0.46 eV bond^{-1}, respectively. Hence, in both compounds, the states just below the Fermi level are mainly from the Nb−Nb and Nb−Sn bonds as well as some Sn−Sn bonding interactions, which suggests that these bonds are significantly contributing to the stability of the compounds.

Both LAPW and LMTO calculations as well as the structural analyses indicate that the covalent characters of Nb−Nb, Nb−Sn, and Sn−Sn bonds are greater than those of RE−Nb and RE−Sn (RE = Sc, Y) bonds. Relatively, the Sc and Y atoms mainly act as spacers and show greater electron-donor character, whereas the Nb atom mainly shows substantial participation in the overall 3D network along with the Sn atoms. Hence, the structures of "$Sc_2Nb_4Sn_5$" and YNb_6Sn_6 can be considered as 3D [Nb_4Sn_5] and [Nb_6Sn_6] anionic frameworks, with RE atoms mainly as cations, respectively.

■ CONCLUSIONS

In summary, we have successfully obtained a series of new ternary rare-earth niobium stannides, namely, $Sc_2Nb_{4-x}Sn_5$ (x = 0.37, 0.52), YNb_6Sn_6, and $ErNb_6Sn_5$ of V_6Si_5-, $HfFe_6Ge_6$- and $LiFe_6Ge_5$-type structures, respectively. Their structures all feature a 3D network based on Nb−Nb, Nb−Sn, and Sn−Sn

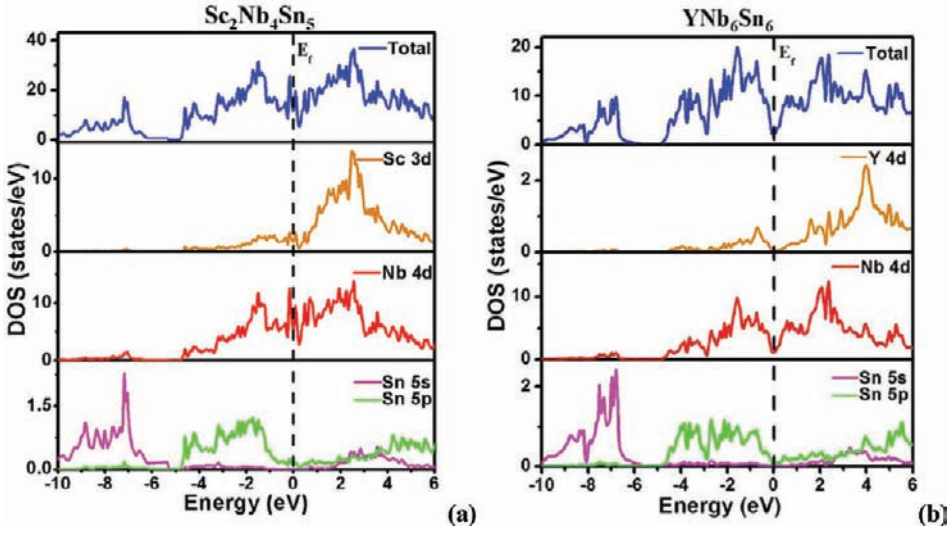

Figure 8. Calculated total and partial DOS for "$Sc_2Nb_4Sn_5$" (a) and YNb_6Sn_6 (b). Contributions from different atoms are color-coded. The Fermi level is set at 0 eV.

dx.doi.org/10.1021/ic202414h | *Inorg. Chem.* 2012, 51, 2461−2471

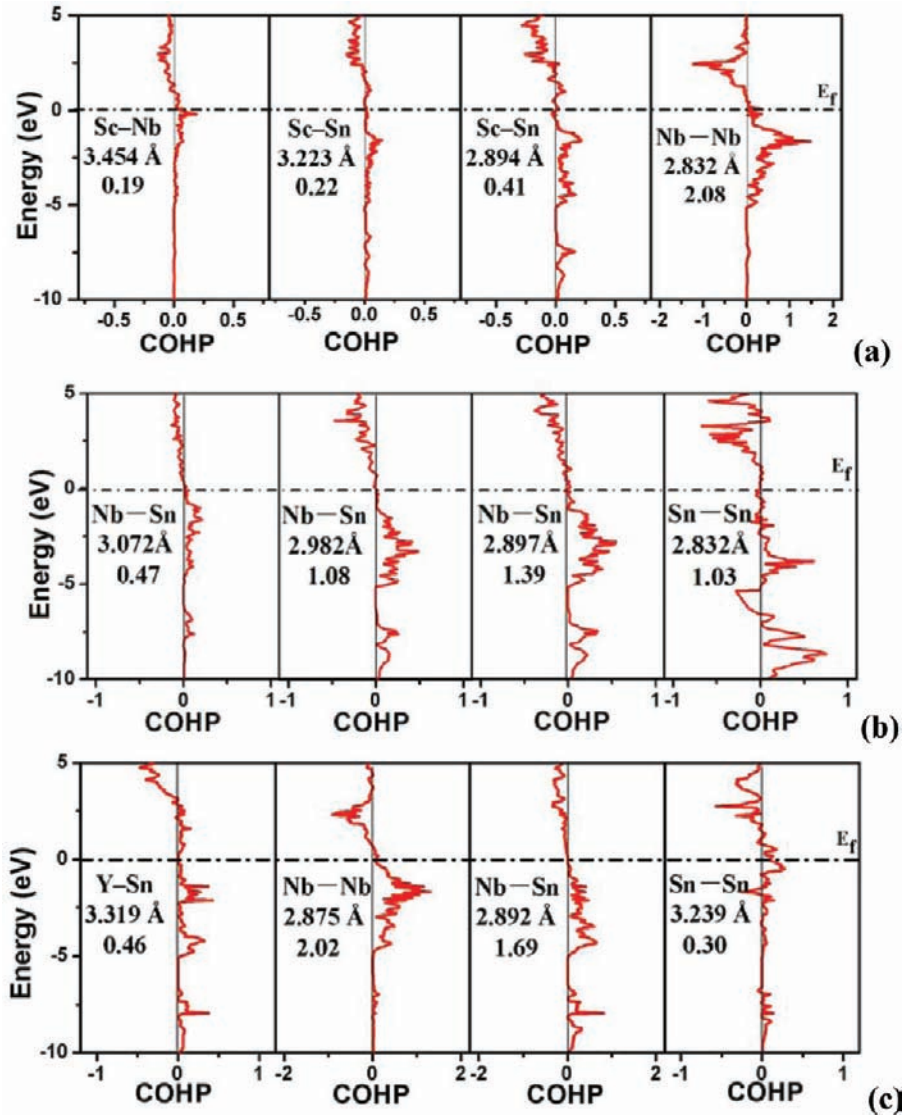

Figure 9. Selected COHP curves for "$Sc_2Nb_4Sn_5$" (a and b) and YNb_6Sn_6 (c). The ICOHP values per bond up to the Fermi level (dotted line) and the corresponding distances are given.

bonds. These compounds further illustrate the effect of transitional metals on the structure type formed. Further research efforts will be devoted to other physical properties, such as the transport and thermoelectric properties of these compounds.

■ ASSOCIATED CONTENT

Ⓢ Supporting Information

Tables of data collection and refinement parameters for $Sc_2Nb_{4-x}Sn_5$ (x = 0.52), anisotropic displacement parameters, and selected bond lengths and the corresponding ICOHP values, figures showing the coordination geometries around RE, Nb, and Sn atoms, the 3D structures of compounds based on various 2D slabs, molar magnetic susceptibilities, and simulated and experimental XRD patterns, and X-ray crystallographic files for all compounds in CIF format. This material is available free of charge via the Internet at http://pubs.acs.org.

■ AUTHOR INFORMATION

Corresponding Author

*E-mail: leixw@fjirsm.ac.cn.

■ ACKNOWLEDGMENTS

We are thankful for financial support from the National Nature Science Foundation of China (Grants 21101075 and 20573113), the Research Foundation for Excellent Young and Middle-aged Scientists of Shandong Province (Grant BS2011CL009), the Science & Research Program Foundation of High Education of Shandong Province (Grant J11LB52), the Rehearsal National Foundation of Jining University (Grants 2011YYJJ06 and 2011YYJJ07), and the Youths Science Foundation of Jining University (Grant 2011QNKJ07).

■ REFERENCES

(1) (a) Corbett, J. D. *Angew. Chem., Int. Ed.* **2000**, *39*, 670. (b) Kanatzidis, M. G.; Poeppelmeier, K. R. *Prog. Solid State Chem.* **2007**, *36*, 1.

(2) (a) Lupu, C.; Mao, J.-G.; Rabalais, J. W.; Guloy, A. M. *Inorg. Chem.* **2003**, *42*, 3765. (b) Fässler, T. F.; Hoffmann, S. *Inorg. Chem.* **2003**, *42*, 5474.

(3) (a) Klem, M. T.; Vaughey, J. T.; Harp, J. G.; Corbett, J. D. *Inorg. Chem.* **2001**, *40*, 7020. (b) Hoffmann, S.; Fässler, T. F. *Inorg. Chem.* **2003**, *42*, 8748.

dx.doi.org/10.1021/ic202414h | *Inorg. Chem.* 2012, 51, 2461–2471

(4) (a) Bobev, S.; Sevov, S. C. *J. Solid State Chem.* **2000**, *153*, 92. (b) Bobev, S.; Sevov, S. C. *Angew. Chem., Int. Ed.* **2000**, *39*, 4108.
(5) (a) Bobev, S.; Sevov, S. C. *J. Am. Chem. Soc.* **2002**, *124*, 3359. (b) Ge, M.-H.; Corbett, J. D. *Inorg. Chem.* **2007**, *46*, 4138.
(6) (a) Nolas, G. S.; Chakoumakos, B. C.; Mahieu, B.; Long, G. J.; Weakley, T. J. R. *Chem. Mater.* **2000**, *12*, 1947. (b) Wilkinson, A. P.; Lind, C.; Young, R. A.; Shastri, S. D.; Lee, P. L.; Nolas, G. S. *Chem. Mater.* **2002**, *14*, 1300.
(7) Leon-Escamilla, E. A.; Corbett, J. D. *Inorg. Chem.* **1999**, *38*, 738.
(8) (a) Pöttgen, R. *Z. Naturforsch.* **2006**, *61b*, 677. (b) Skolozdra, R. V. Stannides of the rare-earth and transition metals. In *Handbook on the Physics and Chemistry of Rare Earths*; Gschneidner, K. A., Eyring, L., Eds.; Elsevier: Amsterdam, The Netherlands, 1997; Vol. *24*, p 164.
(9) (a) Sreeraj, P.; Hoffmann, R.-D.; Wu, Z.-Y.; Pöttgen, R. *Chem. Mater.* **2005**, *17*, 911. (b) Lupu, C.; Downie, C.; Guloy, A. M.; Albright, T. A.; Mao, J.-G. *J. Am. Chem. Soc.* **2004**, *126*, 4386.
(10) (a) Niepmann, D.; Pöttgen, R.; Künnen, B.; Kotzyba, G.; Mosel, B. D. *Chem. Mater.* **2000**, *12*, 533. (b) Niepmann, D.; Pöttgen, R.; Künnen, B.; Kotzyba, G.; Rosenhahn, C.; Mosel, B. D. *Chem. Mater.* **1999**, *11*, 1597. (c) Matar, S. F.; Pöttgen, R.; Huppertz, H. *Intermetallics* **2012**, *20*, 33.
(11) (a) Pöttgen, R.; Hoffmann, R.-D.; Müllmann, R.; Mosel, B. D.; Kotzyba, G. *Chem.—Eur. J.* **1997**, *3*, 1852. (b) Hoffmann, R.-D.; Pöttgen, R.; Kussmann, D.; Müllmann, R.; Mosel, B. D. *Chem. Mater.* **2001**, *13*, 4019.
(12) (a) Sun, Z.-M.; Xia, S.-Q.; Huang, Y.-Z.; Wu, L.-M.; Mao, J.-G. *Inorg. Chem.* **2005**, *44*, 9242. (b) Eul, M.; Langer, T.; Pöttgen, R. *Intermetallics* **2012**, *20*, 98. (c) Wu, Z.-Y.; Hoffmann, R.-D.; Johrendt, D.; Mosel, B. D.; Eckert, H.; Pöttgen, R. *J. Mater. Chem.* **2003**, *13*, 2561.
(13) (a) Hlukhyy, V.; Eck, S.; Fässler, T. F. *Inorg. Chem.* **2006**, *45*, 7408. (b) Mydosh, J. A.; Strydom, A. M.; Baenitz, M.; Chevalier, B.; Hermes, W.; Pöttgen, R. *Phys. Rev. B* **2011**, *83*, 054411.
(14) (a) Matar, S. F.; Chevalier, B.; Isnard, O.; Etourneau, J. *J. Mater. Chem.* **2003**, *13*, 916. (b) Kaczorowski, D.; Gofryk, K.; Romaka, L.; Mudryk, Y.; Konyk, M.; Rogl, P. *Intermetallics* **2005**, *13*, 484. (c) Zhuravleva, M. A.; Bilc, D.; Mahanti, S. D.; Kanatzidis, M. G. *Z. Anorg. Allg. Chem.* **2003**, *629*, 327.
(15) (a) Hlukhyy, V.; Raif, F.; Claus, P.; Fässler, T. F. *Chem.—Eur. J.* **2008**, *14*, 3737. (b) Romaka, V. V.; Gladyshevskii, R.; Gorelenko, Y. *J. Alloys Compd.* **2008**, *453*, L8.
(16) (a) Lei, X.-W.; Zhong, G.-H.; Hu, C.-L.; Mao, J.-G. *J. Alloys Compd.* **2009**, *485*, 124. (b) Pani, M.; Manfrinetti, P.; Palenzona, A.; Dhar, S. K.; Singh, S. *J. Alloys Compd.* **2000**, *299*, 39.
(17) (a) Schreyer, M.; Fässler, T. F. *Solid State Sci.* **2006**, *8*, 793. (b) Schreyer, M.; Kraus, G.; Fässler, T. F. *Z. Anorg. Allg. Chem.* **2004**, *630*, 2520.
(18) (a) Okudzeto, E. K.; Thomas, E. L.; Moldovan, M.; Young, D. P.; Chan, J. Y. *Physica B* **2008**, *403*, 1628. (b) Matar, S. F.; Rodewald, U. C.; Heying, B.; Pöttgen, R. *Solid State Sci.* **2011**, *13*, 1285. (c) Mishra, T.; Schwickert, C.; Langer, T.; Pöttgen, R. *Z. Naturforsch.* **2011**, *66b*, 664.
(19) Lei, X.-W.; Hu, C.-L.; Mao, J.-G. *J. Solid State Chem.* **2010**, *183*, 2032.
(20) (a) Dascoulidou, A.; Schucht, F.; Jung, W.; Schuster, H.-U. *Z. Anorg. Allg. Chem.* **1998**, *624*, 119. (b) Xia, S.-Q.; Bobev, S. *Acta Crystallogr.* **2006**, *E62*, i7.
(21) (a) Manfrinetti, P.; Pani, M. *J. Alloys Compd.* **2005**, *393*, 180. (b) Demchenko, P.; Bodak, O. *J. Alloys Compd.* **2000**, *307*, 215.
(22) (a) Sebastian, C. P.; Fehse, C.; Eckert, H.; Hoffmann, R.-D.; Pöttgen, R. *Solid State Sci.* **2006**, *8*, 1386. (b) Sebastian, C. P.; Zhang, L.; Fehse, C.; Hoffmann, R.-D.; Eckert, H.; Pöttgen, R. *Inorg. Chem.* **2007**, *46*, 771. (c) Sebastian, C. P.; Eckert, H.; Rayaprol, S.; Hoffmann, R.-D.; Pöttgen, R. *Solid State Sci.* **2006**, *8*, 560.
(23) Mishra, R.; Pöttgen, R.; Hoffmann, R.-D.; Trill, H.; Mosel, B. D.; Piotrowski, H.; Zumdick, M. F. *Z. Naturforsch.* **2001**, *56b*, 589.
(24) (a) Cornelius, A. L.; Christianson, A. D.; Lawrence, J. L.; Fritsch, V.; Bauer, E. D.; Sarrao, J. L.; Thompson, J. D.; Pagliuso, P. G. *Physica B* **2006**, *378*−*380*, 113. (b) Christianson, A. D.; Gardner, J. S.; Kang, H. J.; Chung, J.-H.; Bobev, S.; Sarrao, J. L.; Lawrence, J. M. *J. Magn. Magn. Mater.* **2007**, *310*, 266. (c) Sokolov, D. A.; Aronson, M. C.; Henderson, C.; Kampf, J. W. *Phys. Rev. B* **2007**, *76*, 075109. (d) Doniach, S. *Physica B* **1997**, *91*, 231.
(25) (a) Takayanagi, S.; Sato, H.; Fukuhara, T.; Wada, N. *Physica B* **1994**, *199*−*200*, 49. (b) Nagoshi, C.; Sugawara, H.; Aoki, Y.; Sakai, S.; Kohgi, M.; Sato, H.; Onimaru, T.; Sakakibara, T. *Physica B* **2005**, *359*−*361*, 248. (c) Niepmann, D.; Pöttgen, R.; Poduska, K. M.; DiSalvo, F. J.; Trill, H.; Mosel, B. D. *Z. Naturforsch.* **2001**, *56b*, 1.
(26) (a) Gamża, M.; Schnelle, W.; Ślebarski, A.; Burkhardt, U.; Gumeniuk, R.; Rosner, H. *J. Phys.: Condens. Matter* **2008**, *20*, 395208. (b) Thomas, E. L.; Lee, H.-O.; Bankston, A. N.; MaQuilon, S.; Klavins, P.; Moldovan, M.; Young, D. P.; Fisk, Z.; Chan, J. Y. *J. Solid State Chem.* **2006**, *179*, 1641.
(27) (a) Okamoto, H. *J. Phase Equilib.* **2003**, *24*, 380. (b) Westbrook, J. H.; Fleischer, R. L. *Intermetallic Compounds: Principles and Practice*; Wiley: New York, 2002.
(28) Oshchapovsky, L.; Pavlyuk, V.; Fässler, T. F.; Hlukhyy, V. *Acta Crystallogr.* **2010**, *E66*, i82.
(29) (a) *CrystalClear*, version 1.3.5; Rigaku Corp.: Woodlands, TX, 1999. (b) Sheldrick, G. M. *SHELXTL, Crystallographic Software Package*, version 5.1; Bruker-Axs: Madison, WI, 1998.
(30) (a) Madsen, G. K. H.; Blaha, P.; Schwarz, K.; Sjöstedt, E.; Nordström, L. *Phys. Rev. B* **2001**, *64*, 195134. (b) Schwarz, K.; Blaha, P.; Madsen, G. K. H. *Comput. Phys. Commun.* **2002**, *147*, 71. (c) Perdew, J. P.; Burke, K.; Ernzerhof, M. *Phys. Rev. Lett.* **1996**, *77*, 3865. (d) Blaha, P.; Schwarz, K.; Madsen, G. K. H.; Kvasnicka, D.; Luitz, J. In *WIEN2k, An Augmented Plane Wave + Local Orbitals Program for Calculating Crystal Properties*; Schwarz, K., Ed.; Technische Universität: Wien, Austria, 2001.
(31) Blöchl, P. E.; Jepsen, O.; Andersen, O. K. *Phys. Rev. B* **1994**, *49*, 16223.
(32) Anisimov, V. I.; Zaanen, J.; Andersen, O. K. *Phys. Rev. B* **1991**, *44*, 943.
(33) (a) Tank, R. W.; Jepsen, O.; Burkhardt, A.; Andersen, O. K. *TB-LMTO-ASA*, version 4.7; Max-Planck-Institut für Festkörperforschung: Stuttgart, Germany, 1998. (b) Barth, U. V.; Hedin, L. *J. Phys. (Paris)* **1972**, *C5*, 1629. (c) Lambrecht, W. R. L.; Andersen, O. K. *Phys. Rev. B* **1986**, *34*, 2439.
(34) Koelling, D. D.; Harmon, B. N. *J. Phys. (Paris)* **1977**, *C10*, 3107.
(35) (a) Andersen, O. K.; Saha-Dasgupta, T. *Phys. Rev. B* **2000**, *62*, R16219. (b) Tank, R. W.; Arcangeli, C. *Phys. Status Solidi B* **2000**, *217*, 89. (c) Pavarini, E.; Yamasaki, A.; Nuss, J.; Andersen, O. K. *New J. Phys.* **2005**, *7*, 188.
(36) (a) Kotur, B. Y.; Sikirica, M. *J. Less-Common Met.* **1982**, *83*, L29. (b) Steinmetz, J.; Roques, B. *J. Less-Common Met.* **1977**, *52*, 247. (c) Crerar, S. J.; Mar, A. *J. Solid State Chem.* **2004**, *177*, 2523.
(37) Pauling, L.; Kamb, B. *Proc. Natl. Acad. Sci. U.S.A.* **1986**, *83*, 3569.
(38) (a) Lei, X.-W.; Zhong, G.-H.; Li, M.-J.; Mao, J.-G. *J. Solid State Chem.* **2008**, *181*, 2448. (b) Sun, Z.-M.; Pan, D.-C.; Lei, X.-W.; Mao, J.-G. *J. Solid State Chem.* **2006**, *179*, 3378. (c) Lei, X.-W.; Sun, Z.-M.; Li, L.-H.; Zhong, G.-H.; Hu, C.-L.; Mao, J.-G. *J. Solid State Chem.* **2010**, *183*, 920.
(39) (a) Lefèvre, C.; Venturini, G.; Malaman, B. *J. Alloys Compd.* **2003**, *354*, 47. (b) Mazet, T.; Isnard, O.; Malaman, B. *Solid State Commun.* **2000**, *114*, 91.
(40) (a) Gieck, C.; Schreyer, M.; Fässler, T. F.; Cavet, S.; Claus, P. *Chem.—Eur. J.* **2006**, *12*, 1924. (b) Schobinger-Papamantellos, P.; Rodriguez-Carvajal, J.; Buschow, K. H. J. *J. Alloys Compd.* **1997**, *256*, 92.
(41) Eisenmann, B.; Schäfer, H. *Z. Anorg. Allg. Chem.* **1974**, *403*, 163.
(42) Sebastian, C. P.; Eckert, H.; Fehse, C.; Wright, J. P.; Attfield, J. P.; Johrendt, D.; Rayaprol, S.; Hoffmann, R.-D.; Pöttgen, R. *J. Solid State Chem.* **2006**, *179*, 2376.
(43) Cenzual, K.; Gelato, L. M.; Penzo, M.; Parthé, E. *Z. Kristallogr.* **1990**, *193*, 217.
(44) Pearson, W. B. *The crystal chemistry and physics of metals and alloys*; Wiley-Interscience: New York, 1972.

(45) (a) Lei, X.-W.; Zhong, G.-H.; Li, L.-H.; Hu, C.-L.; Li, M.-J.; Mao, J.-G. *Inorg. Chem.* **2009**, *48*, 2526. (b) Lei, X.-W. *J. Solid State Chem.* **2011**, *184*, 852.
(46) (a) Tkachuk, A. V.; Mar, A. *J. Solid State Chem.* **2007**, *180*, 2298. (b) Hoffmann, R.-D.; Pöttgen, R. *Chem.—Eur. J.* **2000**, *6*, 600.